

# Collision-free Path Planning on Arbitrary Optimization Criteria in the Latent Space through cGANs

Tomoki Ando<sup>1</sup>, Hiroto Iino<sup>1</sup>, Hiroki Mori<sup>1,4</sup>, Ryota Torishima<sup>2</sup>,  
Kuniyuki Takahashi<sup>3</sup>, Shoichiro Yamaguchi<sup>3</sup>, Daisuke Okanohara<sup>3</sup>, Tetsuya Ogata<sup>1</sup>

**Abstract**—We propose a new method for collision-free path planning using Conditional Generative Adversarial Networks (cGANs) to transform between the robot joint space and a latent space that captures only collision-free areas of the joint space, conditioned by an obstacle map. When manipulating a robot arm, it is convenient to generate multiple plausible trajectories for further selection. Additionally, it is necessary to generate a trajectory that avoids collision with the robot itself or the surrounding environment for safety reasons. In the proposed method, various trajectories to avoid obstacles can be generated by connecting the start and goal state with arbitrary line segments in this generated latent space. Our method provides this collision-free latent space after which *any* planner, using *any* optimization conditions, can be used to generate the most suitable paths on the fly. We successfully verified this method with a simulated and actual UR5e 6-DoF robotic arm. We confirmed that different trajectories can be generated depending on the choice of optimization conditions.<sup>5</sup>

## I. INTRODUCTION

Collision-free path planning is an essential capability for robots to work in various environments. There are multiple (potentially infinite) paths from a given start to a goal, and it is necessary to choose the optimal path depending on the environment and user requirements (i) *Customizability*. Depending on the application, we may want to perform path planning not only to avoid collision-obstacles, but also to satisfy other criteria such as the efficiency of the robot's movements and/or the speed of its movements. There are other two important factors in collision-free path planning: ii) *Adaptability* and iii) *Scalability of computation*. ii) Robots need to adapt quickly to a new environment, which requires appropriate path planning for the placement to untrained obstacles. iii) These path planning operations should be calculable, even when there is a large number of obstacles, since it generally takes a long time to collision-check for obstacles. In other words, calculation time should scale well with the number of obstacles.

It is challenging to meet these three requirements using existing methods (see Section II). Contrary to traditional

<sup>1</sup>T. Ando, H. Iino, H. Mori, and T. Ogata are with Waseda Univ. & AIST. tomokia@fuji.waseda.jp, {iino, mori}@idr.ias.sci.waseda.ac.jp, ogata@waseda.jp <sup>2</sup>R. Torishima is with SoftBank Corp. This work was an achievement while he was at Waseda Univ. & AIST. ryota.torishima@gmail.com <sup>3</sup>K. Takahashi, S. Yamaguchi, and D. Okanohara are with Preferred Networks. {takahashi, guguchi, hillbig}@preferred.jp <sup>4</sup>H. Mori was a researcher in Cergy-Pontoise Univ. when he came up with the idea.

<sup>5</sup>An accompanying video is available at the following link: <https://www.youtube.com/watch?v=bZTbWxLt6Bo>

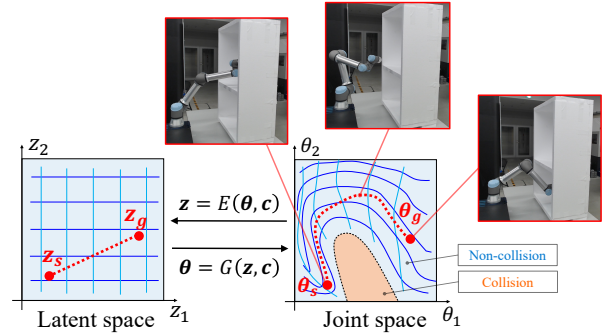


**Fig. 1:** Collision-free path planning for robot arm using latent space of cGANs. Latent variables  $z_s$  and  $z_g$  that correspond to the start  $\theta_s$  and goal  $\theta_g$  joint angles of the robot arm. Any path in the latent space  $z_{s:g}$  is mapped to a collision-free path in the joint space  $\theta_{s:g}$  by using Generator  $G$  with condition  $c$  as obstacle information. On the other hand,  $E$  is an inverse transformation of the Generator  $G$ , in which the joint angles maps to the latent variables.

planning in Cartesian or joint space, we propose to plan trajectories within a new collision-free space as follows. Our method consists of two steps: 1) acquisition of a latent space, and 2) path planning using this latent space. Conditional Generative Adversarial Networks (cGANs) are used to map its latent space to only the collision-free areas of the robot joint space, such that the robot does not collide with obstacles if a path is planned within this latent space (See Fig. 1). That is, selecting any point in the latent space yields a certain robot pose that does not collide with obstacles. There are several methods for acquiring a latent space. We use GANs since there is the advantage that the distribution of the latent space can be arbitrarily determined. By using a uniform distribution of  $[0, 1]$  as the latent space, the domain can be clearly defined and it is a convex space. The mappings from the latent space to joint space *adapts* to various environments by changing according to obstacle information that are given to the cGANs as conditions. The latent space is collision-free and any point on a line connecting any two points is also within this latent space (since this is a convex space). Thus, a collision-free path can be generated by connecting the start and goal states with any arbitrary line or curve in the latent space within a domain of definition. Then, the joint trajectory corresponding to the trajectory planned in latent space is acquired through the learned mappings. Since we separated the learning of the mappings and the actual path planning (or trajectory including optimizations), we can generate **any** trajectory we want on the fly, for **any** optimization parameters that we want

without considering collisions, making our method highly *customizable*. Furthermore, since path planning is performed in the latent space without colliding with obstacles, there is no need collision-check for obstacles. Thus, the computation time does not depend on the number of obstacles, making it *scalable* for complex environments. The most advantage in comparison with existing methods is *customizability*, where trajectories satisfying arbitrary optimisation criteria can be easily generated in this latent space. The adaptability of trajectory generation to changes in the environment and the computational time for the 6-DoF robot were also evaluated, showing the potential for future expansion.

## II. RELATED WORK

There are mainly two types of path planning methods: model-based and learning-based methods. The following two model-based methods are the most common: Design functions for obstacles and goals (e.g., potential fields [1], [2] and Riemannian motion policies with improved potential fields [3]), search and optimization (e.g. RRTs [4]–[6] and  $A^*$  [7]). Methods which are a combination of these are also proposed and generally show improved results [8]–[12]. While model-based methods can reliably avoid obstacles, their adaptability to various environments in real-time is limited since these methods require specific function design and adjustment of parameters for each situation in advance, not to mention the huge computational searching cost. In addition, sometimes certain conditions need to be optimized depending on the purpose, such as the shortest traveling distance in end-effector space or joint space [13] or minimum jerk change [14]; usually multiple or infinite paths for the same start and goal states exist, each of them optimized for different purposes. As model-based methods are usually calculated according to certain conditions/criteria in advance, other calculations need to be performed when these criteria change. In other words, **model-based methods lack scalability and customizability**. The data collected by the model-based methods can be used to train learning-based algorithms, particularly deep learning [15]–[22]. These algorithms can infer a path for a new environment in a short time if it has trained sufficiently in advance. However, learning-based methods have the challenge that only one or a few paths can be generated, and what kind of paths are generated depends on the training data. For example, if naive RRT is used as training data, only collision-free paths to the goal will be generated during inference, usually without taking any additional constraints into account that naive RRT also does not. Usually, **learning-based methods lack customizability**.

In [23], [24], the authors studied the generation of multiple trajectories. Since the target of [23] was to generate various trajectories in environments with no obstacles, obstacle avoidance was out of their scope. Our proposed method is to plan paths in a **collision-free space** which are mapped from the latent space to joint space. Since the trajectory of [24] is fixed once it is generated, at best, only the optimal trajectory among the ones generated can be selected, which is not

necessarily the best for the situation at hand. Thus, they have to generate trajectories until one of them satisfies the criteria necessary for the situation, but they are generated randomly and the method does not provide a way to define optimality. To address this issue, our method does not directly output the trajectories, but simply provides a collision-free space after which any planner, using any optimization conditions, can be used to generate **the most suitable paths**.

The contribution of this research is to realize optimized path planning with the three important factors; i ) *Customizability*, ii ) *Adaptability* , and iii ) *Scalability of computation*.

## III. METHOD

Our proposed method consists of the following two steps: 1) Acquisition of a latent space corresponding to the joint space to avoid collision for *Adaptability* (Section III-A), and 2) path planning according to the objective using the acquired latent space for *Customizability* and *Scalability of computation* (Section III-B.1).

### A. Training cGANs

We propose a method that maps the latent space of cGANs to the collision-free area of the robot joint space, so that the robot learns not to collide with obstacles. Thus, any planned path in that latent space can be associated with a collision-free path in joint space. The mapping from the latent space to joint space *adapts* accordingly to the obstacle information given to cGANs as conditions. The correspondence from the latent space to joint space is trained by cGANs, which uses a min-max game between a Generator  $G$  and a Discriminator  $D$ . Also, Encoder  $E$  is trained to be close to an inverse transformation of  $G$ ; i.e.  $E$  is trained to be equivalent to  $G^{-1}$ .

$$\min_{G,E} \max_D V(D, G, E)$$

These models are optimized alternately with the following objective function with coefficients  $\lambda$ s of each  $\mathcal{L}$ :

$$V(D, G, E) = \lambda_{\text{GAN}} \mathcal{L}_{\text{GAN}}(D, G) + \lambda_{\text{rec}} \mathcal{L}_{\text{rec}}(G, E) + \lambda_{\text{map}} \mathcal{L}_{\text{map}}(G) + \lambda_{\text{col}} \mathcal{L}_{\text{col}}(D) \quad (1)$$

- 1)  $\mathcal{L}_{\text{GAN}}$ : The main loss function to learn the mapping from the latent space to joint space.
- 2)  $\mathcal{L}_{\text{rec}}$ : The loss function to constrain latent space and joint space so that they can be reconstructed with each other.
- 3)  $\mathcal{L}_{\text{map}}$ : The loss function to constrains the transformation from the latent space to the joint space to be smooth.
- 4)  $\mathcal{L}_{\text{col}}$ : The loss function to learn various obstacle situations even if the collision data is a small number in the whole including non-collision data.

The detail of four  $\mathcal{L}$ s will be explained in the following Section III-A.1 through Section III-A.4.

1)  $\mathcal{L}_{\text{GAN}}$ : *Acquisition of Latent Expression*: To acquire the correspondence from the latent space to joint space, cGANs are used. In GANs [25], latent expressions are

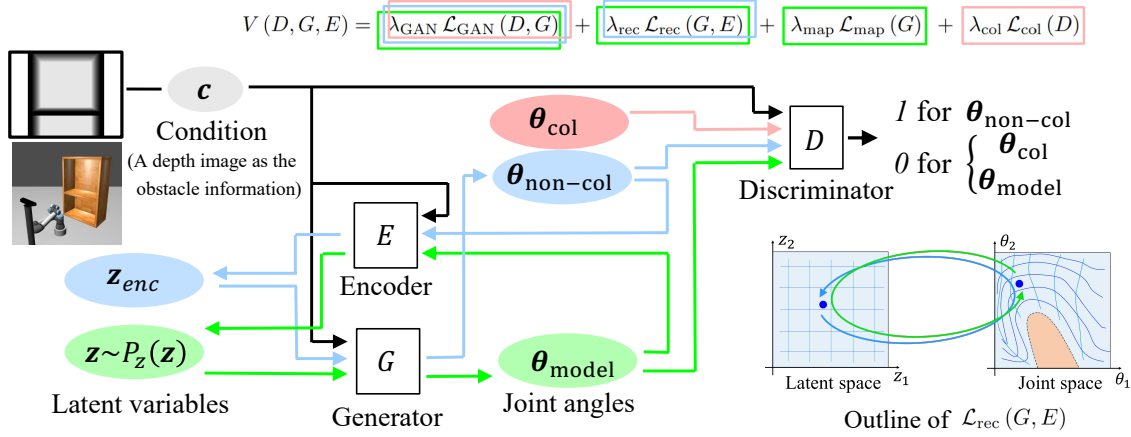


**Fig. 2:** Structure of collision-free path planning model using cGANs. The correspondence between the latent space and joint space is obtained by cGANs. Generator  $G$  transforms the latent variables into collision-free joint angles and Discriminator  $D$  is trained to distinguish between the joint angles generated by Generator  $G$  and those in the dataset. Encoder  $E$  is trained simultaneously as an inverse transformation of Generator  $G^{-1}$ .

acquired by training two models, a Generator  $G$  and a Discriminator  $D$ , alternately. The Generator  $G$  creates data variables  $\theta_{\text{model}}$  from latent variables  $z$ . The Discriminator  $D$  estimates whether given variables are a sample from the data set  $\theta_{\text{non-col}}$  or a generated sample  $\theta_{\text{model}}$  calculated from  $z$ , which is uniformly sampled from the latent space within  $[0, 1]$ . Since the latent space is a convex space and the boundaries of the latent space can be arbitrarily determined in advance, any point of a line segment connecting any point is in that latent space, within a domain of definition. Furthermore, it is possible to give conditions to the models by introducing a *Condition* variable  $c$  [26]. In our case,  $c$  is a depth image as the obstacle information.

Fig. 2 shows the concept of the proposed network model. Through the Generator  $G$ , the mapping from the latent space to collision-free joint space is obtained. The Discriminator  $D$  identifies the joint angles, generated joint angles  $\theta_{\text{model}}$  by the Generator  $G$ , and the actual sampled joint angles  $\theta_{\text{non-col}}$ . In condition  $c$ , the obstacle information is given as a depth image. This condition  $c$  is connected to the Generator  $G$  and the Discriminator  $D$ , so that when the given obstacle information changes, the correspondence from the latent space to joint space changes. In other words, our method does not need to prepare a different network for each obstacle, and only one cGANs can support multiple obstacle environments. The loss function,  $\mathcal{L}_{\text{GAN}}$ , for training cGANs is shown in equation (2).

$$\begin{aligned} \mathcal{L}_{\text{GAN}}(D, G) = & \mathbb{E}_{c \sim p_{\text{obs}}(c), \theta \sim p_{\text{non-col}}(\theta|c)} [\log D(\theta, c)] \\ & + \mathbb{E}_{c \sim p_{\text{obs}}(c), z \sim p_z(z)} [\log (1 - D(G(z, c), c))] \end{aligned} \quad (2)$$

Where  $p_{\text{obs}}(c)$  is the distribution of obstacles positions and  $p_{\text{non-col}}(\theta|c)$  is the distribution of non-collision joint angles which the Generator should aim to generate.  $p_z(z)$  is the uniform distribution in the latent space.

2)  $\mathcal{L}_{\text{rec}}$ : *Reconstruction of latent variables and joint angles*: This section describes an objective function that constrains the latent space and joint space so that they can be reconstructed from each other. In this method, given a

start and a goal in the joint space, it is necessary to obtain the corresponding latent variables in the latent space. The transformation from the latent space to joint space can be trained by  $\mathcal{L}_{\text{GAN}}$ , but the transformation from the joint space to latent space requires the inverse transformation of the Generator  $G^{-1}$ . However, if there is a point where multiple points in the latent space correspond to a single point in the joint space, the inverse transformation cannot exist. Therefore, Encoder  $E$  is trained simultaneously as an inverse transformation of Generator  $G^{-1}$  and simultaneously learning the reconstruction of the latent space and the joint space, so that the each point in the joint space and latent space correspond one-to-one (constrain the Generator  $G$  to be a single projection). This loss function,  $\mathcal{L}_{\text{rec}}$ , is shown in equation (3).

$$\begin{aligned} \mathcal{L}_{\text{rec}}(G, E) \\ = & \mathbb{E}_{c \sim p_{\text{obs}}(c), \theta \sim p_{\text{non-col}}(\theta|c)} [\|G(E(\theta, c), c) - \theta\|_2^2] \\ & + \mathbb{E}_{c \sim p_{\text{obs}}(c), z \sim p_z(z)} [\|E(G(z, c), c) - z\|_2^2] \end{aligned} \quad (3)$$

3)  $\mathcal{L}_{\text{map}}$ : *Specifying the Map from the Latent Space to Joint Space*: We will describe in this section how to map from the latent space to joint space, such that arbitrary planned paths in the latent space are smooth in joint space for robot arms. In equation (2), the path planned in the latent space is mapped from each point in the latent space to joint space, but it is not certain whether the path planned in the latent space can be realized by the robot in joint space. For the purpose of path planning using a robot arm, the mapping from the latent space to joint space has to be continuous without “twists”, “distortions”, and rapid changes. In order to achieve this, the following two things are performed:

- The number of dimensions for latent variables is matched to the number of robot joints; each latent variable is mapped to represent each joint, and the normalized ranges of latent variables and joint angles are aligned.

- The Generator  $G$  is trained to output  $\theta$  when the latent variables  $z = \theta$  are given as input of the Generator  $G$ . In other words, a certain distance in the latent space is almost the same distance in joint space.

However, since the acquired map may be distorted in order to avoid collisions, these constraints are not added to the joint that collides with the obstacles. The loss function,  $\mathcal{L}_{\text{map}}$ , for training cGANs is shown in equation (4).

$$\mathcal{L}_{\text{map}}(G) = \mathbb{E}_{c \sim p_{\text{obs}}(c), \theta \sim p_{\text{non-col}}(\theta|c)} [\|G(z = \theta, c) - \theta\|_2^2] \quad (4)$$

4)  $\mathcal{L}_{\text{col}}$ : *Adaptability to Multiple Obstacle Conditions*: In this section, we describe how to adapt to various obstacle conditions. Even though collision-free mapping from the latent space to joint space is trained by equation (2), the network cannot learn well since the number of non-collision data points is much smaller than those with collisions. As the obstacles become more diverse, there is a risk of mistaking collision points for non-collision points and vice versa.

It is therefore necessary to train with the collision joints explicitly incorporated within the equation. The loss function,  $\mathcal{L}_{\text{col}}$ , shown in equation (5) is introduced in order to provide the data of the collision joints to the Discriminator  $D$ .

$$\mathcal{L}_{\text{col}}(D) = \mathbb{E}_{c \sim p_{\text{obs}}(c), \theta \sim p_{\text{col}}(\theta|c)} [\log(1 - D(\theta, c))] \quad (5)$$

Where  $p_{\text{col}}(\theta|c)$  is the distribution of colliding joint angles including self-collision and collide with obstacles, which the Generator  $G$  should thus refrain from generating. The Discriminator  $D$  is trained to output 0 for collision joints and 1 for collision-free joints for each obstacle. Furthermore, the Generator  $G$  is trained to acquire a distribution to make the Discriminator  $D$  output 1, as we are trying to obtain a distribution for collision-free space.

## B. Path Planning

In this section we will describe the path planning method. Section III-B.1 describes how to generate various optimal trajectories for different purposes, and Section III-B.2 explains how to guarantee collision avoidance with obstacles, since learning methods alone cannot completely avoid collisions with obstacles.

1) *Optimal Path Trajectory Generation*: Unlike traditional path planners in joint space, since the mapping and path planning phases are separated, any path planner can be used in the trained latent space (where any point is collision-free) without taking obstacles into account since there simply are none in the latent space, making our method highly *customizable*. As optimization methods for any optimization criterion, we can use not only any discrete optimization methods such as  $A^*$  [7] on any graphs in the latent space but also continuous optimization methods such as Adam [27] thanks to the differentiable nature of the Generator  $G$ . The computational cost is also lower since collision check calculations are no longer necessary, making our method also *scalable*.

As shown in Fig. 1, when the start joint angles  $\theta_s$  and the goal joint angles  $\theta_g$  are given, the corresponding latent

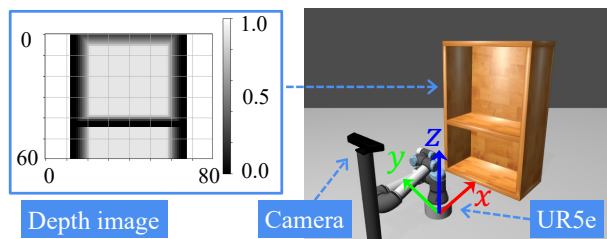


Fig. 3: Experiment environment and depth image of obstacle.

variables are found by  $z_s = E(\theta_s, c)$ ,  $z_g = E(\theta_g, c)$ . Considering  $z_{s:t}$  as a path connecting these in the latent space, the collision-free path is obtained as  $\theta_{s:t} = G(z_{s:t}, c)$ .

$z_{s:t}$  can be determined arbitrarily within the latent space, and in the simplest case, it can be simply connected by a straight line. Taking advantage of the differentiability of the Generator  $G$ , the path in the latent space can be calculated by optimizing the cost function  $\mathcal{L}_{\text{opt}}$  to satisfy the objective using the following equation:

$$\begin{aligned} \mathcal{L}_{\text{opt}} &= f(G, z_{s:g}, c) \\ \hat{z}_{s:g} &= \underset{z_{s:g}}{\text{argmin}} \mathcal{L}_{\text{opt}} \end{aligned} \quad (6)$$

There are a variety of cost functions depending on the objectives. For example,  $\mathcal{L}_{\text{opt}}$  can be minimization of the sum of squares of velocities  $\mathcal{L}_{\text{opt}} = \sum_t \|\mathbf{v}_t\|_2^2$ , minimization of acceleration  $\mathcal{L}_{\text{opt}} = \sum_t \|\mathbf{a}_t\|_2^2$ , and minimization of jerk  $\mathcal{L}_{\text{opt}} = \sum_t \|\mathbf{j}_t\|_2^2$ , where  $\mathbf{v}_t = \theta_t - \theta_{t-1}$ ,  $\mathbf{a}_t = \mathbf{v}_t - \mathbf{v}_{t-1}$ , and  $\mathbf{j}_t = \mathbf{a}_t - \mathbf{a}_{t-1}$ . Also, the path can be optimized by combining them as the following equation:

$$\mathcal{L}_{\text{opt}} = \sum_t \|\mathbf{v}_t\|_2^2 + \alpha \sum_t \|\mathbf{a}_t\|_2^2 + \beta \sum_t \|\mathbf{j}_t\|_2^2 \quad (7)$$

2) *Collision Avoidance Guarantee (CAG)*: We will describe a method to guarantee collision avoidance. The learning method does not guarantee 100% obstacle avoidance. Therefore, the trajectory obtained by the Generator  $G$  is checked to ensure that it does not collide with any obstacles, and if a colliding posture is found, the trajectory is modified to guarantee collision avoidance. If the path includes a colliding posture, the non-colliding posture before and after the collision trajectory is modified using existing path planning methods. In this study, we used RRT Connect [5].

## IV. EXPERIMENTAL SETUP

We performed experiments using a Gazebo simulation and real 6-DoF UR5e robot arm. In learning-based methods using robotic arms in 3-D space, objects like pillars or shelves are often used as obstacles. We use a shelf for tasks that are closer to practical applications. We set up an environment with a shelf in front of the robot as an obstacle, and evaluate the performance of the system under multiple conditions by changing the obstacle position of the shelf and the height of the center plate of the shelf (Fig. 3). The origin of the coordinate system is the floor just below the root of the robot, with the forward direction in the positive  $x$ -axis, the left side in the positive  $y$ -axis, and the upper side in the positive  $z$ -axis. The robot is placed on a 10 cm high pedestal.

## A. Data Collection

1) *Robot Information*: The datasets of cGANs consists of 6 joint angles  $\theta = (\theta_1, \theta_2, \theta_3, \theta_4, \theta_5, \theta_6)$  that represents the posture of the robot. The ranges of the joint angles are  $\theta_1 \in [-90^\circ, 90^\circ]$ ,  $\theta_2 \in [-120^\circ, 120^\circ]$ ,  $\theta_i \in [-180^\circ, 180^\circ]$  ( $i = 3, 4, 5, 6$ ). The latent variables  $z$  are 6-dimensional because the robot has 6-DoF, and a uniform distribution in the range  $[0, 1]$  is used.

2) *Obstacle Information*: The size of the shelf to be placed as an obstacle is 120 cm in height, 80 cm in width, and 40 cm in depth. The shelf is placed in various locations, which are divided into 5 positions by  $x \in [60 \text{ cm}, 70 \text{ cm}]$  and 9 positions by  $y \in [-10 \text{ cm}, 10 \text{ cm}]$ , and the shelf is located so that the training data and test data alternated. Similarly, the height of the board is divided into 11 parts in the range  $z \in [50 \text{ cm}, 60 \text{ cm}]$  so that the training data and test data alternate. Therefore, there are  $23 (\text{positions}) \times 6 (\text{heights}) = 138$  different types of condition for training data, and  $22 (\text{positions}) \times 5 (\text{heights}) = 110$  different types of condition for test data.

By random sampling, we collected a total of 50,000 collision and non-collision data of robot postures for various obstacle conditions, and used them for training. The percentage of collision data is about 43% of the total. The breakdown is: self collision and floor collision (about 37%) and shelf collision (about 9%). Note that in some cases both collisions occur at the same time, so the total exceeds 43%. Min-Max scaling was applied to each of  $\theta_i$ , and they were normalized to the range of  $[0, 1]$ .

For the condition  $c$  that indicates the obstacle information, we used a depth image taken from behind the robot. The depth image is taken in such a way that the robot is not included in the image, and one depth image corresponds to each obstacle condition. The depth image is a one-channel image with a size of  $60 \times 80$  pixels. The shelf is placed in the  $[40 \text{ cm}, 90 \text{ cm}]$  range on the x-axis, and the depth information is normalized by  $[0, 1]$  in that range.

## B. Network Design

Our network model is composed of  $G$ ,  $D$  and  $E$  with fully connected layers, and each network includes a two-dimensional convolutional layer (conv.) as a feature extraction unit for Conditions  $c$  (Fig. 2). The details of the network design are shown in Table I. For learning stabilization, batch normalization [28] are spectral normalization [29] were used. Our network model is implemented with PyTorch, a deep learning library. Training is conducted on a machine equipped with Intel Core i7-11700F@2.50GHz CPU and GeForce RTX 3070, resulting in about 3 to 4 days of training time.

We describe  $\lambda_s$ , which are the coefficients of each loss function in the equation (1). They are set as  $\lambda_{\text{GAN}} = 1$ ,  $\lambda_{\text{rec}} = 100$ ,  $\lambda_{\text{map}} = 10$ , and  $\lambda_{\text{col}} = 100$ . When the distance between the robot and the obstacle is less than 10cm,  $\lambda_{\text{rec}} = 0$  and  $\lambda_{\text{map}} = 0$  are used. If the robot collides with the shelf,  $\lambda_{\text{col}} = 1000$ . The purpose of this is to increase safety by ensuring the distance to collision, Generator  $G$  is trained to

TABLE I: Network design

	Layer	In	Out	Filter size	Norma- lization	Activation function
Conv <sup>1</sup>	1 <sup>st</sup> conv.	1	4	(3,3)	BN	Leaky ReLU
	2 <sup>nd</sup> conv.	4	4	(3,3)	BN	Leaky ReLU
	AvgPool1	4	4	(2,2)	-	-
	3 <sup>rd</sup> conv.	4	8	(3,3)	BN	Leaky ReLU
	4 <sup>th</sup> conv.	8	8	(3,3)	BN	Leaky ReLU
	AvgPool2	8	8	(2,2)	-	-
	5 <sup>th</sup> conv.	8	16	(3,3)	BN	Leaky ReLU
	AvgPool3	16	16	(2,2)	-	-
	FC <sub>obs-0</sub>	1120	1024 <sup>2</sup>	-	BN	Leaky ReLU
	FC <sub>obs-1</sub>	1024 <sup>2</sup>	1024 <sup>3</sup>	-	BN	Leaky ReLU
FC <sub>obs-2</sub>	1024 <sup>2</sup>	1024 <sup>3</sup>	-	BN	Leaky ReLU	
FC <sub>obs-3</sub>	1024 <sup>2</sup>	1024 <sup>3</sup>	-	BN	Leaky ReLU	
D	1 <sup>st</sup> FC	6	256	-	-	Leaky ReLU
	2 <sup>nd</sup> FC	256	512	-	SN	Leaky ReLU
	3 <sup>rd</sup> FC	512	1024 <sup>3</sup>	-	SN	Leaky ReLU
	4 <sup>th</sup> FC	1024	1024 <sup>3</sup>	-	SN	Leaky ReLU
	5 <sup>th</sup> FC	1024	1024 <sup>3</sup>	-	SN	Leaky ReLU
	6 <sup>th</sup> FC	1024	1024	-	SN	Leaky ReLU
	7 <sup>th</sup> FC	1024	1024	-	SN	Leaky ReLU
	8 <sup>th</sup> FC	1024	1	-	-	Linear
G &† E	1 <sup>st</sup> FC	6	256	-	-	Leaky ReLU
	2 <sup>nd</sup> FC	256	512	-	SN	Leaky ReLU
	3 <sup>rd</sup> FC	512	1024 <sup>3</sup>	-	SN	Leaky ReLU
	4 <sup>th</sup> FC	1024	1024 <sup>3</sup>	-	SN	Leaky ReLU
	5 <sup>th</sup> FC	1024	1024 <sup>3</sup>	-	SN	Leaky ReLU
	6 <sup>th</sup> FC	1024	1024	-	SN	Leaky ReLU
	7 <sup>th</sup> FC	1024	1024	-	SN	Leaky ReLU
	8 <sup>th</sup> FC	1024	6	-	-	Linear

<sup>1</sup>  $G$ ,  $D$ , and  $E$  have independent feature extraction units.

<sup>2</sup> The output of FC<sub>obs-0</sub> is the input to FC<sub>obs-1</sub>, FC<sub>obs-2</sub>, and FC<sub>obs-3</sub>, respectively.

<sup>3</sup> The element-wise product of the output of FC<sub>obs-1</sub> and the output of 3<sup>rd</sup> FC is the input to the next layer. The same process applies to the outputs of FC<sub>obs-2</sub> and 4<sup>th</sup> FC, and to the outputs of FC<sub>obs-3</sub> and 5<sup>th</sup> FC.

<sup>4</sup>  $G$  and  $E$  have the same structure but independent parameters.

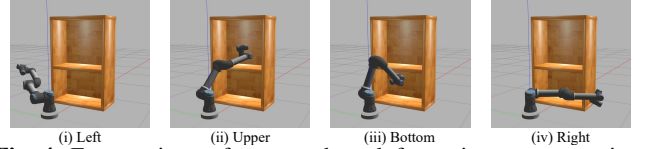


Fig. 4: Four regions of start and goal for trajectory generation: left, upper, bottom, and right relative to the shelf. Random postures were set as the start and the goal from two different regions among them.

exclude postures that are close to obstacles.

## C. Settings for the Comparison Methods

The Python implementation in ROS was used for the RRT Connct [5] used in the proposed method and for the RRT [4] and RRT\* [8] used for comparison with the proposed method. We used the default parameters of the motion planning framework MoveIt!.

## V. EXPERIMENT RESULTS

We will confirm the ii) **Adaptability** to various obstacles by evaluating the acquired mapping in section V-A. Next, i) **Customizability** will be confirmed by path planning on several optimization criteria in section V-B, and iii) **Scalability** will be confirmed by comparison with other path planning methods in section V-C and collision avoidance guarantee will be verified. Finally, we show results with a real robot, UR5e in section V-D.

### A. Evaluation of Adaptability to Various Obstacles

We evaluate the accuracy of the mapping acquired as  $G$  and  $E$  by evaluation of success rate of path planing to verify ii) **Adaptability**. For the evaluation, random postures were set as the start and the goal from two different regions among

**TABLE II:** Success rate of path planning. Path planning was performed by connecting straight lines in latent space for a given start and goal. Note that the collision avoidance guarantee (CAG) is not used in the path planning of any method.

	$\mathcal{L}_{\text{map}}$	$\mathcal{L}_{\text{col}}$	Dataset	Path Success Rate [%]
Ours	w	w	Train	72.7 (85.3)
			Test	70.9 (89.4)
w/o $\mathcal{L}_{\text{map}}$	w/o	w	Train	22.9 (24.2)
			Test	15.8 (20.0)
w/o $\mathcal{L}_{\text{col}}$	w	w/o	Train	17.6 (31.9)
			Test	17.0 (32.1)

the regions whose end-effector positions were *left*, *upper*, *bottom*, and *right* relative to the shelf (Fig. 4). Then, for various obstacle conditions as described in Section IV-A.2, we let the robot arm’s end-effector plan a path to cross the shelf board using the above start and goal posture. Note that the posture of the robot arm at the start and goal is at least 5 cm away from the collision. For each obstacle condition, three paths are generated;  $138 \text{ conditions} \times 3 \text{ paths} = 414 \text{ paths}$  are evaluated for train datasets, and  $110 \text{ conditions} \times 3 \text{ paths} = 330 \text{ paths}$  are evaluated for test datasets. Although there are several possible paths in the latent space, we use the path that connects the two points by a straight line in the latent space after calculating  $\mathbf{z}_s = E(\boldsymbol{\theta}_s, \mathbf{c})$  and  $\mathbf{z}_g = E(\boldsymbol{\theta}_g, \mathbf{c})$  using the inverse transform of the generator,  $E$ , for the start and goal postures  $\boldsymbol{\theta}_s$  and  $\boldsymbol{\theta}_g$ , respectively. The length of  $\mathbf{z}_{s:g}$  is fixed at 200 steps.

The definition of success in path planning is that the generated path does not contain any collision postures and that the start and goal positions are reached. The method for determining whether the start and goal positions have been reached is to calculate the Euclidean distance difference of  $(x, y, z)$  between the end-effector position calculated from given start and goal postures and the reconstructed start and goal postures from the latent variables generated by path planning as follows:

$$\|FK(\boldsymbol{\theta}_{\text{rec}}) - FK(\boldsymbol{\theta}_{\text{target}})\| < \epsilon \quad (8)$$

where,  $FK()$  is forward kinematics to calculate end-effector position from  $\boldsymbol{\theta}$ ,  $\boldsymbol{\theta}_{\text{rec}} = G(E(\boldsymbol{\theta}_{\text{target}}, \mathbf{c}), \mathbf{c})$ , and  $\epsilon = 5.0 \text{ cm}$ .

In this experiment, we verify the effectiveness of each loss of the proposed method. Our proposed method consists of four loss functions, as shown in equation (1). Since  $\mathcal{L}_{\text{GAN}}$  and  $\mathcal{L}_{\text{rec}}$  are the minimum required for the training of the model, the following three conditions are used to examine the effectiveness of the other  $\mathcal{L}$ s: (a) Our proposed method, (b) without  $\mathcal{L}_{\text{map}}$  from equation (1), and (c) without  $\mathcal{L}_{\text{col}}$  from equation (1). Note that the collision avoidance guarantee (CAG) is not used in the path planning of any method.

Table II shows the results of the experiment. The success rates shown in brackets in Table II include those that were able to generate trajectories without collisions with obstacles, but did not satisfy equation (8), i.e. failed to reconstruct. Table II shows that the success rate drops significantly without either  $\mathcal{L}_{\text{map}}$  or  $\mathcal{L}_{\text{col}}$ . Since the path success rate is low even when failure of reconstruction is taken into account,

**TABLE III:** Evaluation of the optimized trajectory

Target to optimize	$\sum_t \ \mathbf{v}_t\ _2^2$	$\sum_t \ \mathbf{a}_t\ _2^2$	$\sum_t \ \mathbf{j}_t\ _2^2$
w/o Opt.	$1.16 \pm 0.21$	$0.20 \pm 0.12$	$0.38 \pm 0.27$
$\mathbf{v}$	<b><math>0.75 \pm 0.25</math></b>	$0.055 \pm 0.012$	$0.11 \pm 0.032$
$\mathbf{a}$	$1.06 \pm 0.29$	<b><math>0.031 \pm 0.014</math></b>	$0.033 \pm 0.024$
$\mathbf{j}$	$1.17 \pm 0.23$	$0.052 \pm 0.017$	<b><math>0.026 \pm 0.010</math></b>
Mix of $\mathbf{v}, \mathbf{a}, \mathbf{j}$	$0.92 \pm 0.25$	$0.042 \pm 0.011$	$0.049 \pm 0.016$

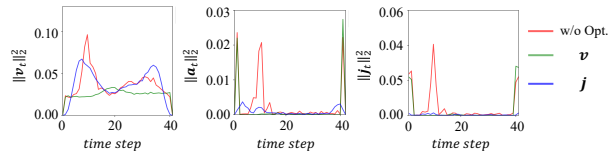


**Fig. 5:** The values  $\mathbf{v}, \mathbf{a}, \mathbf{j}$  of before and after optimization. The trajectory before optimization is generated by connecting the latent space with a straight line. The trajectory is optimized by velocity minimization and jerk minimization, respectively.

it can be said that a large rate of collisions with obstacles occurs in trajectory.

We also confirmed that the success rate decreased by 18.5% when a depth image different from actual obstacle information was provided to the condition. We provided the depth image where the shelf was placed at  $x = 63 \text{ cm}$ ,  $y = 0 \text{ cm}$  and the board was placed at  $z = 55 \text{ cm}$ . From the results, we confirmed that the generated paths varied depending on the conditions. The proposed method has a high success rate of more than 70% for both train dataset and test dataset, indicating that it can generate trajectories even under untrained obstacle conditions. In other words, the *adaptability* of the proposed method to various obstacle conditions is verified.

### B. Path Planning on Arbitrary Optimization Criteria

In this section, we verify i) *Customizability*. The proposed method can generate multiple (in-finite) paths. No matter what kind of path is planned in the latent space, the result is mapped to the corresponding collision-free path in joint space. The method for determining paths in the latent space is not limited to just connecting the start and the goal linearly, but can be any path/trajectory planner.

As examples of optimization, Table III shows the values of the trajectories before and after optimization when velocity  $\mathbf{v}$ , acceleration  $\mathbf{a}$ , and jerk  $\mathbf{j}$  are minimized, and combination are performed as described in Section III-B.1. The hyperparameters in the combination of optimization were set to  $\alpha = 0.5$  and  $\beta = 0.5$  in equation (7). The 330 trajectories (110 untrained conditions  $\times$  3 pairs of start and goal) from the test dataset used in Section V-A are used as the trajectories before optimization. Of these trajectories, only those that avoided obstacles before and after optimization were used to generate the results in Table III. The results of guaranteeing obstacle avoidance will be shown in Section V-C. From the Table III, it can be confirmed that the value subjected to each optimization is the smallest. These optimizations took approximately 2 s to 10 s, and latent variables were updated from 500 to a maximum 2,500 iterations.

As an example of trajectory optimization, Fig. 5 shows the values of  $\mathbf{v}, \mathbf{a}$ , and  $\mathbf{j}$  before optimization, which is just a straight line in the latent space, and the trajectory after opti-

**TABLE IV: Success rate and execution time for path planning<sup>1</sup>**

Start-Goal	Method	Success Rate [%]	Planning Time [ms]	Path Length [m]
Left-Upper	Ours w/o CAG	68.3	5.95 ± 0.16	1.48 ± 0.21
	Ours (only CAG)	100.0	114.35 ± 90.10	1.73 ± 0.50
	Ours	100.0	40.32 ± 71.02	1.56 ± 0.34
	RRT	100.0	419.16 ± 1305.27	2.03 ± 0.59
	RRT Connect	100.0	119.16 ± 2.54	2.26 ± 0.88
Left-Bottom	Ours w/o CAG	70.2	5.95 ± 0.17	1.91 ± 0.36
	Ours (only CAG)	100.0	6.02 ± 0.25	1.97 ± 0.50
	Ours	100.0	5.97 ± 0.20	1.93 ± 0.40
	RRT	100.0	473.35 ± 1144.82	2.77 ± 1.47
	RRT Connect	100.0	126.48 ± 7.71	2.43 ± 0.97
Left-Right	Ours w/o CAG	81.8	5.94 ± 0.15	3.00 ± 0.39
	Ours (only CAG)	100.0	35.53 ± 54.79	2.78 ± 0.43
	Ours	100.0	11.32 ± 24.94	2.96 ± 0.40
	RRT	100.0	201.96 ± 254.73	2.81 ± 0.80
	RRT Connect	100.0	125.20 ± 2.41	3.14 ± 1.46
Upper-Bottom	Ours w/o CAG	69.4	5.95 ± 0.16	1.11 ± 0.27
	Ours (only CAG)	100.0	89.17 ± 149.75	1.42 ± 0.78
	Ours	100.0	31.45 ± 90.07	1.20 ± 0.50
	RRT	98.4	1264.04 ± 3315.85	1.88 ± 1.05
	RRT Connect	100.0	128.10 ± 30.49	2.03 ± 0.90
Upper-Right	Ours w/o CAG	73.2	5.94 ± 0.13	1.64 ± 0.32
	Ours (only CAG)	100.0	76.23 ± 59.47	1.37 ± 0.56
	Ours	100.0	24.77 ± 43.44	1.57 ± 0.41
	RRT	100.0	377.65 ± 651.56	1.78 ± 0.69
	RRT Connect	100.0	118.71 ± 2.22	1.93 ± 0.71
Bottom-Right	Ours w/o CAG	66.3	5.92 ± 0.12	1.91 ± 0.48
	Ours (only CAG)	100.0	112.90 ± 274.59	2.65 ± 1.19
	Ours	100.0	42.02 ± 165.55	2.16 ± 0.86
	RRT	97.5	854.78 ± 2119.77	2.44 ± 1.51
	RRT Connect	100.0	136.42 ± 78.67	2.16 ± 1.17

<sup>1</sup> The execution time is calculated only for path planning and does not include the GPU transfer time (about 10 ms)

mization by velocity minimization and jerk minimization, respectively. The trajectory before optimization has some parts where the velocity and jerk change suddenly. By optimizing the trajectory with velocity minimization, the velocity of the entire trajectory is suppressed. In the trajectory optimized by jerk minimization, the sudden stops and starts at the start and goal are moderated. Since the values of the graphs generated by each optimization are different, we can say that different trajectories were generated as a result of the optimization.

These results show that path planning can be performed using arbitrary optimization criteria, which demonstrates the *customizability* of our proposed method.

### C. Comparison of the Planning Times and Collision Avoidance Guarantee

Here, we investigate iii) *Scalability* and collision avoidance guarantee (CAG). We evaluate the success rate and computation time of the proposed method (which use CAG by RRT Connect if collision occurs when planning with cGANs) using the 330 (110 untrained conditions × 3 pairs of start and goal) used in Section V-A. In addition to our method without CAG, the model-based path planning methods RRT and RRT Connect are used for comparison. Since the trajectories generated by RRT and RRT Connect are different each time, three trials are conducted with the same start, goal and obstacle conditions. As well as, the proposed method uses RRT Connect, therefore, three trials are conducted. To investigate the computation time when RRT Connect is used for the CAG of the proposed method, we denote as Ours (only CAG) the success rate and computation time when CAG is used for the data whose path planning fails in Ours w/o CAG. Note that this success rate and computation time do not include the success rate and computation time when Ours w/o CAG succeeds. These results are shown in Table IV. The success rate is the same

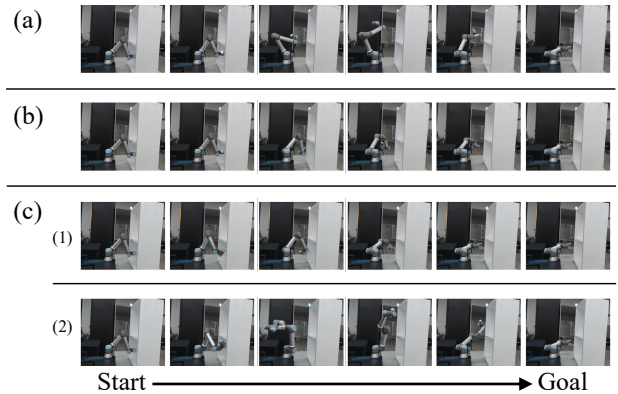


**Fig. 6: Demonstration on a real robot.** Different trajectories were generated for (a) to (c). (a) Ours without trajectory optimization, (b) Ours using trajectory optimization by speed minimization, (c) Generated trajectories using RRT Connect.

as Section V-A, which is the percentage of trajectories that do not collide with any obstacles and satisfy equation (8). Note that for the RRT and RRT Connect methods, if the execution time exceeded 60 s, the method was counted as a failure to find a path.

Ours w/o CAG is a path planning in the latent space where there is no collision with obstacles, so the computation time is almost constant, independent of the complexity of the environment. However, learning-based methods alone cannot guarantee 100% collision avoidance with obstacles. In our results, the success rate of learning a trajectory without contact with obstacles was more than 60%. Even though the RRT and RRT Connect methods achieve a high success rate, these methods require more computation time as the complexity of the environment increases, because the collision check is required each time. Furthermore, the trajectory generated by each trial is different each time. In particular, when the complexity of the environment increases, the variance of generated trajectories becomes larger. In this experiment, it was shown that the variance of the computation time and the length of the generated path is large for the *Upper-Bottom* and *Bottom-Right* paths. Our method uses RRT Connect to compute the trajectory only before and after the collision. Thus, the computation time is less than that of RRT or RRT Connect, which requires collision check in all trajectories, as shown in Ours (only CAG). The average computation time for Ours is  $27.67 \pm 96.15$  ms in total, which is 21.8% of that for RRT Connect of  $126.79 \pm 44.84$  ms. While generating a single trajectory may result in collisions with obstacles in our method, generating multiple different trajectories, such as using different optimization criteria, or selection of different trajectories in the latent space, can also reduce the likelihood of using RRT Connect. Therefore, our proposed method requires even less computation time than RRT and RRT Connect. These indicate that the computational cost of our method is *scalable* to the complexity of the environment.

### D. Experiments Using UR5e

In this section, we show the results of experiments using a real UR5e. Using the model trained with the simulation

dataset, UR5e performed path planning. The shelf was placed at the same position as in the simulator, and the depth information was the same as in the simulator for the image. In the experiments, we used (a) Ours without trajectory optimization, (b) Ours using trajectory optimization by speed minimization, and (c) Generated trajectories using RRT Connct. Fig. 6 shows the generated trajectories. In (a), we confirm that our proposed method generates collision-free path. In (b), a shorter path is generated by optimizing the speed. In (c), using RRT Connect, the trajectory generated by each trial is different each time. On the other hand, in our method, if the same trajectory is selected in the latent space, the same trajectory will be generated in the joint space.

## VI. CONCLUSION

In this research, the robot's collision-free joint space are expressed as the latent space of cGANs, and collision-free paths are obtained by mapping the path planned in the latent space to joint space. We confirmed that i) **Customizability**; any path can be planned in the latent space using any optimization criteria, ii) **Adaptability**; a single trained model could handle multiple untrained obstacle conditions, and iii) **Scalability**; computational cost of path planning does not depend on the obstacles. By modifying the trajectory in case of a collision when path planning is done by learning alone, 100% collision avoidance can be guaranteed.

## APPENDIX

As a pre-experiment, we have published a paper in arXiv in which a 2-DoF robot arm is tested on a 2-D plane<sup>6</sup>. In the pre-experiment paper, the focus is on analysis because of the small number of DoFs. In this new paper, the model is extended to a 6-DoF robot in 3-D space, but the concept of the model, which maps the non-collision posture to the potential space, is the same.

## ACKNOWLEDGMENTS

H. Mori would like to thank all colleagues in ETIS lab in the Cergy-Pontoise Univ., especially Prof. Mathias Quoy, Prof. Philippe Gaussier and Assoc. Prof. Alexandre Pitti, for discussion about a preliminary result of the basic idea of this article when he came up the basic idea at the lab in 2016.

## REFERENCES

- [1] C. W. Warren, "Multiple robot path coordination using artificial potential fields," in *Proceedings., IEEE International Conference on Robotics and Automation*. IEEE, 1990, pp. 500–505.
- [2] G. Li, *et al.*, "An efficient improved artificial potential field based regression search method for robot path planning," in *2012 IEEE International Conference on Mechatronics and Automation*, 2012, pp. 1227–1232.
- [3] N. D. Ratliff, *et al.*, "Riemannian motion policies," *arXiv preprint arXiv:1801.02854*, 2018.
- [4] S. M. LaValle *et al.*, "Rapidly-exploring random trees: A new tool for path planning," 1998.
- [5] J. J. Kuffner and S. M. LaValle, "RRT-connect: An efficient approach to single-query path planning," in *Proceedings 2000 ICRA. Millennium Conference. IEEE International Conference on Robotics and Automation. Symposia Proceedings (Cat. No. 00CH37065)*, vol. 2. IEEE, 2000, pp. 995–1001.
- [6] S. M. LaValle and J. J. Kuffner Jr, "Randomized kinodynamic planning," *The international journal of robotics research*, vol. 20, no. 5,

- pp. 378–400, 2001.
- [7] P. Hart, *et al.*, "A formal basis for the heuristic determination of minimum cost paths," *IEEE Transactions on Systems Science and Cybernetics*, vol. 4, no. 2, pp. 100–107, 1968. [Online]. Available: <https://doi.org/10.1109/tssc.1968.300136>
- [8] S. Karaman and E. Frazzoli, "Incremental sampling-based algorithms for optimal motion planning," in *Robotics: Science and Systems VI*. MIT Press, 2011, pp. 267–274.
- [9] K. Naderi, *et al.*, "RT-RRT\*: a real-time path planning algorithm based on rrt\*," 11 2015, pp. 113–118.
- [10] A. H. Qureshi and Y. Ayaz, "Intelligent bidirectional rapidly-exploring random trees for optimal motion planning in complex cluttered environments," *Robotics and Autonomous Systems*, vol. 68, pp. 1–11, 2015.
- [11] —, "Potential functions based sampling heuristic for optimal path planning," *CoRR*, vol. abs/1704.00264, 2017. [Online]. Available: <http://arxiv.org/abs/1704.00264>
- [12] Z. Tahir, *et al.*, "Potentially guided bidirectionalized RRT\* for fast optimal path planning in cluttered environments," *Robotics and Autonomous Systems*, vol. 108, pp. 13–27, 2018.
- [13] T. Lalibertk and C. M. Gosselin, "Efficient algorithms for the trajectory planning of redundant manipulators with obstacle avoidance," in *Proceedings of the 1994 IEEE International Conference on Robotics and Automation*, 5 1994, pp. 2044–2049.
- [14] T. Flash and N. Hogan, "The coordination of arm movements: an experimentally confirmed mathematical model," *Journal of Neuroscience*, vol. 5, pp. 1688–1703, 1985.
- [15] A. Srinivas, *et al.*, "Universal planning networks: Learning generalizable representations for visuomotor control," in *International Conference on Machine Learning*. PMLR, 2018, pp. 4732–4741.
- [16] A. Tamar, *et al.*, "Value iteration networks," *CoRR*, vol. abs/1602.02867, 2016. [Online]. Available: <http://arxiv.org/abs/1602.02867>
- [17] B. Ichter, *et al.*, "Learning sampling distributions for robot motion planning," in *2018 IEEE International Conference on Robotics and Automation (ICRA)*. IEEE, 2018, pp. 7087–7094.
- [18] A. Wang, *et al.*, "Learning robotic manipulation through visual planning and acting," *CoRR*, vol. abs/1905.04411, 2019. [Online]. Available: <http://arxiv.org/abs/1905.04411>
- [19] R. Kumar, *et al.*, "Lego: Leveraging experience in roadmap generation for sampling-based planning," *arXiv preprint arXiv:1907.09574*, 2019.
- [20] R. Terasawa, *et al.*, "3d-cnn based heuristic guided task-space planner for faster motion planning," in *2020 International Conference on Robotics and Automation (ICRA)*. IEEE, 2020, pp. 9548–9554.
- [21] K. Ota, *et al.*, "Efficient exploration in constrained environments with goal-oriented reference path," *arXiv preprint arXiv:2003.01641*, 2020.
- [22] S. Wen, *et al.*, "Path planning of humanoid arm based on deep deterministic policy gradient," in *2018 IEEE International Conference on Robotics and Biomimetics (ROBIO)*, 2018, pp. 1755–1760.
- [23] K. Kutsuzawa, *et al.*, "Motion generation considering situation with conditional generative adversarial networks for throwing robots," *arXiv preprint arXiv:1910.03253*, 2019.
- [24] A. H. Qureshi, *et al.*, "Motion planning networks," *CoRR*, vol. abs/1806.05767, 2018.
- [25] I. Goodfellow, *et al.*, "Generative adversarial nets," *Advances in neural information processing systems*, vol. 27, 2014.
- [26] M. Mirza and S. Osindero, "Conditional generative adversarial nets," *CoRR*, vol. abs/1411.1784, 2014. [Online]. Available: <http://arxiv.org/abs/1411.1784>
- [27] D. Kingma and J. Ba, "Adam: A method for stochastic optimization," *International Conference on Learning Representations*, 12 2014.
- [28] S. Ioffe and C. Szegedy, "Batch normalization: Accelerating deep network training by reducing internal covariate shift," in *Proceedings of the 32nd International Conference on Machine Learning - Volume 37, ser. ICML' 15*. JMLR.org, 2015, p. 448–456.
- [29] T. Miyato, *et al.*, "Spectral normalization for generative adversarial networks," in *International Conference on Learning Representations*, 2018.

<sup>6</sup>The link of the article is the following:  
<https://arxiv.org/abs/2202.07203>